

Distributed Model-based Predictive Secondary Control for Hybrid AC/DC Microgrids

Erwin Rute-Luengo, Alex Navas-Fonseca, Juan S. Gómez, Enrique Espina, Claudio Burgos-Mellado, Doris Sáez, *Senior Member, IEEE*, Mark Sumner, *Senior Member, IEEE*, and Diego Muñoz-Carpintero

Abstract—This paper presents a novel scheme based on distributed model-based predictive control for the secondary level control of hybrid AC/DC microgrids. Prediction models based on droop control and power transfer equations are proposed to characterize the generators in both the AC and DC sub-microgrids, whereas power balance constraints are used to predict the behavior of interlinking converters. The operational constraints (such as powers and control action limits) are included in all the formulations. Experimental results validate the proposed scheme for the following cases: (i) load changes, working within operating constraints, (ii) managing frequency regulation in the AC sub-microgrid, voltage regulation in the DC sub-microgrid and global power consensus in the whole hybrid microgrid, and (iii) maintaining the microgrid performance in the presence of communication malfunction while ensuring that plug-and-play capability is preserved.

Index Terms—Microgrids, Hybrid AC/DC Microgrids, Distributed Secondary Control, Predictive Control.

I. INTRODUCTION

Hybrid microgrids (MGs) are composed of an AC-side and a DC-side, known as sub-MGs, joined together by at least one bidirectional interlinking converter (ILC) [1]. AC and DC loads can be connected on each sides, reducing unnecessary conversion stages and increasing the power capacity and the reliability of the entire MG [2].

AC-MGs can operate in both grid-connected and isolated modes. The latter mode is used when the power grid is not available, e.g., in remote/rural areas. In this mode, the control is based on a grid forming/supporting scheme where at least one distributed generator (DG) operates as a voltage source, regulating the MG voltage magnitude and frequency [3]. DC-MGs neither require reactive power control nor frequency regulation, thus reducing the system operational complexity. Moreover, in DC-MGs, the DGs do not need to be synchronized to the utility [1]. Furthermore, the voltage of DG-MGs is affected only by the active power flowing, while in AC-MGs, the voltage can be regulated using reactive power without affecting the active power if the distribution lines are predominantly inductive [4].

This work was supported in part by “Agencia Nacional Investigación y Desarrollo” (ANID) through project ANID/FONDAP/15110019; in part by Instituto Sistemas Complejos de Ingeniería (ISCI) under Grant ANID PIA/BASAL AFB180003; in part by Project VID UChile ENL08/21; in part by ANID/concurso de fomento a la vinculación internacional para instituciones de investigación regionales (modalidad corta duración)/FOVI210023; in part by ANID PIA ACT192013; in part by ANID/PAI 2019-PAI77190021; in part by Secretaría de Educación Superior, Ciencia, Tecnología e Innovación de Ecuador under Grant SENESCYT/ARSEQ-BEC-0058482018; in part by ANID BECAS/DOCTORADO NACIONAL under Grant 2019-21190961; and in part by ANID BECAS/DOCTORADO NACIONAL under Grant 2017-21171858.

The MG control uses a hierarchical control structure to group its control tasks [5]. The primary control level comprises the inner voltage and current loops to control power electronic converters, which are used as interfaces between the DGs and the hybrid AC/DC MG. Outer droop controllers impose the linear relationships between active power-frequency and reactive power-voltage that change the operating point when the AC-MG is disturbed. The DC-MG droop controller changes the voltage according to the active power demanded. In both cases, droop controllers emulate the required system inertia for DGs which use renewable sources [6].

The secondary control level of each DG on the AC sub-MG regulates voltage and frequency, while only voltage is regulated on the DC sub-MG. When distributed control schemes are used, the control action is computed locally by each DG controller, using available information of the MG operation. Information exchange between secondary controllers permits the pursuit of global objectives, e.g., voltage regulation or equitable power-sharing throughout the MG [7], [8]. Distributed control schemes are robust against electrical/communication disturbances and communication malfunction, such as latency or data dropouts. Furthermore, distributed schemes remove the inherent drawbacks of centralized control, such as single point failure and excessive computational burden [9], [10].

For hybrid AC/DC MGs, the power transfer between the AC sub-MG and the DC sub-MG is a paramount control objective. There are two approaches to include this global objective into the control hierarchy [11][2]. The first one states as the control objective, the real-time active power sharing between the AC and DC sub-MGs [12], and it is usually supported only on the primary droop control. The second approach uses active power sharing whenever one sub-MG is overloaded [13]; this is usually done through optimal control-based strategies, penalizing the power transfer through ILCs.

The authors of [12] present a decentralized control strategy to coordinate the power sharing between multiple AC and DC sub-MGs, considering constant power loads and passive loads. This control scheme considers a common DC bus through the whole MG; then, bidirectional AC/DC and DC/DC converters act as ILCs. Weighted relationships between the DC voltages and the AC sub-MG frequency are regulated using Proportional Integral (PI) controllers. The weighting terms used to set these relationships between multiple sub-MGs are based on the power ratings and the critical power loads. However, a better performance could be achieved by coordinating control between the DG units instead of using the decentralized method proposed in [12].

The authors of [13] propose a power management system at the tertiary level, based on mixed-integer linear programming, to optimize the power transfer through the ILC. Ad-hoc models of a wind turbine, a diesel generator, a photovoltaic generator, and a battery bank are set as constraints into the optimization problem. This controller prioritizes the usage of renewable energies over the diesel generator and the battery bank, improving the MG performance and reducing operating costs. A similar approach is reported in [14], where a multi-objective optimization problem, solved using particle swarm optimization, is presented to optimize the operating cost of the MG. In this work, the power transferred between both of the sub-MGs is reduced by penalizing the cost function. However, both approaches [13], [14] are centralized and work at the tertiary control level with a sampling time ranging from minutes to hours. In this case, scalability and plug-and-play characteristics are difficult to implement.

The power transfer control objective of the ILC should be set considering the frequency and voltage behavior of the AC and DC sub-MGs to preserve the MG proper operation, as well as using additional parameters such as the power rating of each DG. In this sense, secondary control schemes such as the distributed averaged proportional-integral (DAPI) control [8], [15], [16], or model-based predictive control (MPC) [7], [17], [18] combine regulation and power sharing objectives for independent AC or DC sub-MGs. The ILC control scheme should be aligned with the secondary control objectives of both sub-MGs. The best way to achieve these objectives is to integrate cooperative power sharing strategies which are not affected by topology changes or communication malfunctions which disturb the hybrid AC/DC MG. In addition, the usual control schemes for ILCs in hybrid MGs set the power transfer at the tertiary control level by centralized or distributed control techniques. To the author's best knowledge, only [19], [20] proposed a DAPI based control strategy for the operation of hybrid AC/DC MGs at the secondary control level. Nevertheless, it has been reported that MPC has better performance when communication delays are present in the communication network when compared to traditional PI techniques [7], [21], [22]. This is because MPC can handle the issues of the communication delay due to its use of a rolling horizon.

For these reasons, this paper proposes a distributed secondary control scheme based on MPC (DMPC) to operate hybrid isolated MGs. DMPC controllers are proposed for AC and DC sub-MGs and for ILCs. They include operating constraints, and power transfer models and avoid using a model of the complete MG, or models of primary source generation (wind, PV, etc.). The DMPC for the ILC pursues equitable active power sharing between the AC sub-MG and the DC sub-MG to distribute the load across the entire MG. The contributions of this paper are as follows:

i) To the best of the author's knowledge, this is the first paper that proposes distributed cooperative predictive controllers for hybrid AC/DC MGs composed of AC sub-MGs, DC sub-MGs and ILCs. The proposed DMPC controllers work cooperatively to manage the hybrid MG as one whole system instead of three separate subsystems. Also, a complete model of the hybrid MG is not required thanks to its distributed

nature.

ii) For the control of the DC sub-MG and the ILCs, novel predictive models and cost functions of both subsystems were developed to implement the proposed DMPC approach. Furthermore, an improved DMPC controller (compared to that reported in [7]) is proposed to control the AC sub-MG. It uses the DMPC discussed in [7] augmented with voltage observers for estimating the voltage downstream of the coupling inductor (Li) (See Fig. 1). This new approach reduces the number of voltages sensors (and implementation cost) of the improved DMPC controller compared with [7]. As a result, the entire control system is robust to communication malfunction and ensures the plug-and-play capability of both DG units (AC and DC) and the ILCs, as demonstrated in sections IV, V and VI.

iii) A DMPC scheme is proposed for the ILCs to transfer active power between the AC sub-MG and the DC sub-MG. Therefore, one side can supply a deficit of active power if the demand on the other side is too high. This DMPC does not interfere with operation of the sub-MG controllers, i.e., frequency and voltage regulation in the AC sub-MG and voltage regulation in the DC sub-MG are preserved. Furthermore, active power is transferred proportionally to the power rating of the ILCs.

iv) For the DC sub-MG, a DMPC is proposed for restoring the average DC voltage to its nominal value and sharing the active power of the DC-DGs proportionally to their power rating. This last objective works in conjunction with the controllers for ILCs and AC-DGs to share active power in the entire hybrid AC/DC MG proportionally to the DGs power rating capacities.

v) Unlike other secondary control schemes proposed for hybrid AC/DC MGs [19], [20], based on DAPI controllers, the proposed DMPC scheme can achieve multiple control objectives while incorporating physical operating constraints of the hybrid AC/DC MG, such as, maximum power rating limits of not only DGs but also ILCs, and output voltage limits. As a result, more control objectives can be achieved with fewer control actions when compared with traditional DAPI based controllers [19].

vi) The proposed DMPC approach for hybrid AC/DC MGs has a better dynamic response under communication time delays in the communication network than previously reported works based on DAPI controllers [19], [20]. This superior behavior is due to the rolling horizon property of the DMPC method. In section VI, a detailed comparison between the proposed DMPC controller and the DAPI-based technique [19] is presented.

The remainder of this paper is organized as follows. Section II states the framework of the hybrid MG configuration used. Section III-A and Section III-B present the DMPC formulation for the AC sub-MG and the DC sub-MG, respectively. Section III-C explains in detail the DMPC controller for the ILC. Experimental and simulation results are presented in Section IV and Section V, respectively. Section VI highlights the advantages of the proposed DMPC against a reported DAPI-based approach. Finally, conclusions and future research are discussed in Section VII.

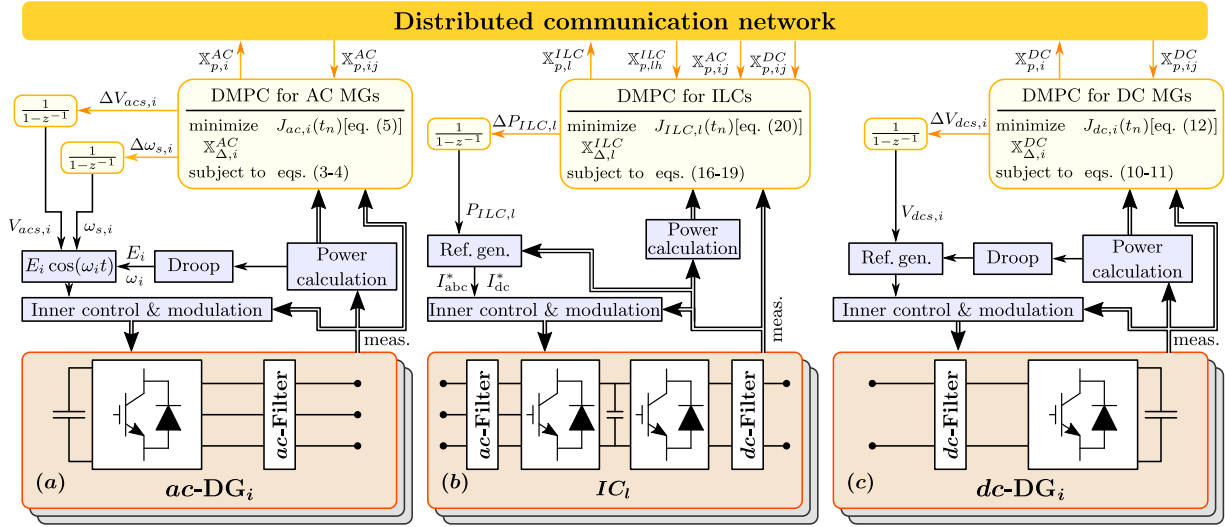


Fig. 1. Proposed DMPC scheme for the control of hybrid AC/DC MGs.

II. MICROGRID CONFIGURATION

In this section, the hybrid MG framework used in this paper is stated. A hybrid MG is considered composed of a set of $N_{ac} + N_{dc} + N_{IL}$ DGs and ILCs. $\mathbb{N}_{ac} = \{1, \dots, N_{ac}\}$ represents the subset of DGs on the AC sub-MG, $\mathbb{N}_{dc} = \{1, \dots, N_{dc}\}$ stands for the subset of DGs on the DC sub-MG and, $\mathbb{N}_{IL} = \{1, \dots, N_{IL}\}$ denotes the subset of ILCs, which connect the AC and DC sub-MGs together. A multi-node MG is considered, so it is not mandatory that the ILCs should be connected to the same node. For this paper, the ILC secondary controllers pursue active power consensus between the AC and DC sub-MGs, whereas local AC and DC secondary controllers ensure active power consensus, preserving frequency and voltage regulation on the AC sub-MG and voltage regulation on the DC sub-MG.

The general control structure for the $AC - DG_i$, ILC_i and $DC - DG_i$ are presented in Fig. 1.a, Fig. 1.b and Fig. 1.c, respectively. These controllers are explained in detail later in Section III. Note that the AC and DC DGs are operating in grid-forming mode, voltage source converters (VSC), as shown in Fig. 1.a and Fig. 1.c, respectively. A coupling impedance is placed between the output filter and the MG, which allows the computation of the power contribution from each DG to the MG. At the AC sub-MG, this impedance is an inductance (L_i), which forms an LCL output filter, whereas for the DC sub-MG it is a resistance (R_i) (see Fig. 2 and Fig. 3, respectively). Whereas in [7] the voltage after the coupling impedance is measured directly using real-time sensors, in this paper, a sensorless approach is used by introducing Ohm's-law based voltage observers, which are defined in Section III-A and Section III-B for the AC and DC sub-MGs, respectively.

Considering that distributed control schemes require information exchange to achieve their cooperative control objectives, a communication network model is used, to include for latency and connectivity phenomena. Latency is defined as the end to end communication delay, which means it is an aggregation of transportation and processing delays. Connectivity is

represented by the $(N_{ac} + N_{dc} + N_{IL}) \times (N_{ac} + N_{dc} + N_{IL})$ adjacency matrix A , where its entries a_{ij} are defined for $i, j \in \mathbb{N}_{ac} \cup \mathbb{N}_{dc} \cup \mathbb{N}_{IL}$ in (1) as a function of the received information on DG_i at the instant t_n .

$$a_{ij}(t_n) = \begin{cases} 1 & \text{Data from } DG_j \text{ arrives to } DG_i \text{ at } t_n \\ 0 & \text{Data from } DG_j \text{ does not arrive to } DG_i \text{ at } t_n \\ 0 & j = i \end{cases} \quad (1)$$

The formulations of the predictive controllers for AC sub-MG, DC sub-MG and ILCs are detailed in next section.

III. DMPC FORMULATION FOR HYBRID AC/DC MICROGRIDS

In this section, the formulations of the DMPCs used for AC-DGs, DC-DGs and ILCs in the hybrid microgrid are described. The DMPC for AC DGs corresponds to an improved version of the proposed technique reported in [7] by some of this paper's authors. The method presented in [7] is augmented with voltage observers, reducing the number of voltage sensors required for its implementation. The method reported in [7] requires measurements of voltage and current at the LC filter and the voltage downstream of the coupling inductor (L_i) (see Fig. 2). In contrast, the improved version proposed in this paper only requires the usual voltage and current measurements at the LC filter, and the voltage upstream L_i is estimated based on [23].

It is worth remembering that the control of a hybrid microgrid comprises the control of three subsystems: (i) AC sub-MG, (ii) DC sub-MG, and (iii) interlinking converters (ILCs). In this paper, the control of the AC sub-MG is achieved by an improved version of the control system reported in [7] and discussed in Section III-A. The proposed DMPC for the DC DGs and the ILCs are described in detail in sections III-B and III-C, respectively. These sections show how the continuous-time models are derived. Discrete-time prediction models are then presented, which are derived using the forward Euler discretization method. For any non-linear models, a Taylor expansion is used to linearize these models.

A. DMPC for AC sub-microgrid

The DMPC scheme used as secondary control in the AC sub-MG regulates the frequency and average voltage to their nominal values (ω_0 and V_{ac0}), and achieves active power consensus, i.e., all DGs contribute to the power-sharing proportionally their nominal power rating as well as reactive power consensus. The set of equations (2) is used to state the prediction model for the i -th AC DG, and describes the $P-\omega$ droop control response (2a), the $Q-V$ droop control response (2b), the phase angle deviation (2c), the active power (2d) and reactive power (2e) transferred from DG_i to the MG. In this case $i \in \mathbb{N}_{ac}$; the secondary control actions are $\omega_{s,i}$ and $V_{acs,i}$. The droop slopes are $M_{p\omega,i}$, and $M_{qv,i}$, and $B_i = 1/(L_i\omega_0)$.

$$\omega_i(t) = \omega_0 + M_{p\omega,i}P_i(t) + \omega_{s,i}(t) \quad (2a)$$

$$V_{ac,i}(t) = V_{ac0} + M_{qv,i}Q_i(t) + V_{acs,i}(t) \quad (2b)$$

$$\delta\theta_i(t) = \theta_i(t) - \hat{\theta}_i^L(t) = \int_0^t [\omega_i(\tau) - \hat{\omega}_i^L(\tau)] d\tau \quad (2c)$$

$$P_i(t) = B_i V_{ac,i}(t) \hat{V}_{ac,i}^L(t) \sin(\delta\theta_i(t)) \quad (2d)$$

$$Q_i(t) = B_i [V_{ac,i}(t)^2 - V_{ac,i}(t) \hat{V}_{ac,i}^L(t) \cos(\delta\theta_i(t))] \quad (2e)$$

Fig. 2 shows the control diagram for the i th AC-DG of the AC sub-MG, where the LCL output filter connected to DG_i is composed of L_{fi} , C_{fi} and L_i . The voltage ($V_{ac,i}$), current ($i_{ac,i}$), frequency (ω_i) and phase angle (θ_i) are measurable/estimable variables at the filter capacitor. Additionally, a reduced-order observer, based on [23], is used to estimate the voltage $\hat{V}_{ac,i}^L$, at the adjacent measurement node downstream of L_i , whereas $\hat{\omega}_i^L$ and $\hat{\theta}_i^L$ are computed by a phase-locked loop (PLL) [24]. The proposed secondary control is, therefore, a multiple input-multiple output DMPC controller.

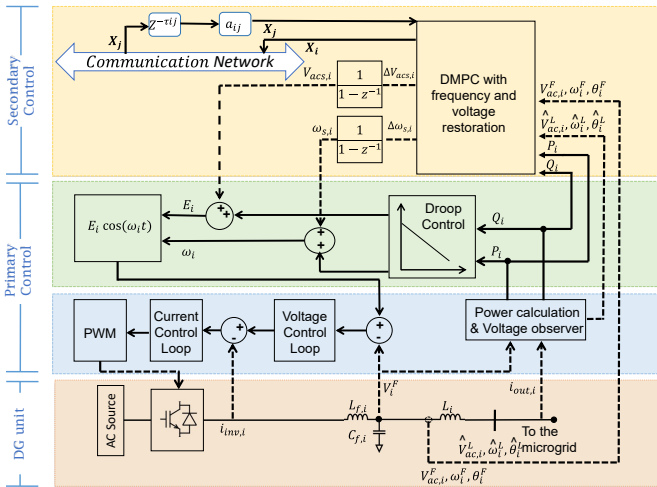


Fig. 2. DMPC_{*i*} Diagram for AC DGs on the AC sub-MG.

The prediction models included as equality constraints into the optimization problem are defined by (3), where

$t_n = nT_{sec}$, $n \in \mathbb{Z}^+$, and T_{sec} is the sampling time of the controller. Furthermore, $\Delta f(t_n) = f(t_n) - f(t_{n-1})$ is defined as the incremental operator, and it is applied in (2a). Hence, the optimization problem is expressed as a function of the control actions variations ($\Delta\omega_{s,i}$ and $\Delta V_{acs,i}$). These predictive models are stated for t_{n+k} steps ahead, where $k \in \mathbb{Z}^+$. The measured/estimated point used for linearization purposes is composed of $\{\omega_i(t_n), \hat{\omega}_i^L(t_n), V_i(t_n), \hat{V}_i^L(t_n), \delta\theta_i(t_n), P_i(t_n)\}$. Note that local approximations of the MG average frequency and average voltage ($\bar{\omega}_i$ and $\bar{V}_{ac,i}$) are used in equations (3f) and (3g) which depend on the communication terms $a_{ij}(t_n)$ and the estimated delay ($\hat{\tau}_{ij}$). The latter is defined as one sampling period at the secondary level. Furthermore, the terminal constraints (3h) and (3i) guarantee the convergence of the DMPC to the nominal frequency and nominal voltage at the end of the prediction horizon N_y [25].

$$\begin{aligned} \omega_i(t_{n+k}) = & \omega_i(t_{n+k-1}) + M_{p\omega,i} [P_i(t_{n+k}) - P_i(t_{n+k-1})] \\ & + \Delta\omega_{s,i}(t_{n+k-1}) \end{aligned} \quad (3a)$$

$$\begin{aligned} V_{ac,i}(t_{n+k}) = & V_{ac,i}(t_{n+k-1}) + M_{qv,i} [Q_i(t_{n+k}) - Q_i(t_{n+k-1})] \\ & + \Delta V_{acs,i}(t_{n+k-1}) \end{aligned} \quad (3b)$$

$$\delta\theta_i(t_{n+k}) = \delta\theta_i(t_{n+k-1}) + T_{sec} [\omega_i(t_{n+k}) - \hat{\omega}_i^L(t_n)] \quad (3c)$$

$$\begin{aligned} P_i(t_{n+k}) = & P_i(t_n) \\ & + [\delta\theta_i(t_{n+k}) - \delta\theta_i(t_n)] B_i V_{ac,i}(t_n) \hat{V}_{ac,i}^L(t_n) \cos(\delta\theta_i(t_n)) \\ & + [V_{ac,i}(t_{n+k}) - V_{ac,i}(t_n)] B_i \hat{V}_{ac,i}^L(t_n) \sin(\delta\theta_i(t_n)) \end{aligned} \quad (3d)$$

$$\begin{aligned} Q_i(t_{n+k}) = & Q_i(t_n) \\ & + [V_{ac,i}(t_{n+k}) - V_{ac,i}(t_n)] B_i [2V_{ac,i}(t_n) - \hat{V}_{ac,i}^L(t_n) \cos(\delta\theta_i(t_n))] \\ & + [\delta\theta_i(t_{n+k}) - \delta\theta_i(t_n)] B_i V_{ac,i}(t_n) \hat{V}_{ac,i}^L(t_n) \sin(\delta\theta_i(t_n)) \end{aligned} \quad (3e)$$

$$\bar{\omega}_i(t_{n+k}) = \frac{\omega_i(t_{n+k}) + \sum_{j \in \mathbb{N}_{ac}} a_{ij}(t_n) \omega_j(t_{n+k} - \hat{\tau}_{ij})}{1 + \sum_{j \in \mathbb{N}_{ac}} a_{ij}(t_n)} \quad (3f)$$

$$\bar{V}_{ac,i}(t_{n+k}) = \frac{V_{ac,i}(t_{n+k}) + \sum_{j=1}^n a_{ij}(t_n) V_{ac,j}(t_{n+k} - \hat{\tau}_{ij})}{1 + \sum_{j=1}^n a_{ij}(t_n)} \quad (3g)$$

$$\bar{\omega}_i(t_{n+N_y}) = \omega_0 \quad (3h)$$

$$\bar{V}_{ac,i}(t_{n+N_y}) = V_{ac0} \quad (3i)$$

In addition, inequality constraints to bound the solution space and improve the transient response of the controller are included. The DG_i 's output voltage is limited in (4a). The active power and reactive power contributions are limited to the power rating S_{max} in (4b). In the same way, the rate of change of the control actions (4c) and (4d) are included.

$$V_{ac,min} \leq V_{ac,i}(t_{n+k}) \leq V_{ac,max} \quad (4a)$$

$$|P_i(t_n)| + |Q_i(t_n)| + \text{sign}(P_i(t_n))[P_i(t_{n+k}) - P_i(t_n)] \\ + \text{sign}(Q_i(t_n))[Q_i(t_{n+k}) - Q_i(t_n)] \leq S_{\max} \quad (4b)$$

$$\Delta\omega_{s,imin} \leq \Delta\omega_{s,i}(t_{n+k-1}) \leq \Delta\omega_{s,imax} \quad (4c)$$

$$\Delta V_{acs,imin} \leq \Delta V_{acs,i}(t_{n+k-1}) \leq \Delta V_{acs,imax} \quad (4d)$$

The cost function (5) is built from six weighted terms which pursuit frequency regulation, a minimum frequency control action variation, active power consensus, average voltage regulation, a minimum voltage control action variation, and reactive power consensus, respectively. Note that the active power consensus and reactive power consensus are updated only with the predicted information of communicated neighboring DG units, and they depend on the communication terms $a_{ij}(t_n)$ and the estimated delay ($\hat{\tau}_{ij}$). The optimization problem composed of (3), (4) and (5) is synthesized as a canonical quadratic programming (QP) problem with linear constraints. The optimization output is composed of the predicted vector $\mathbb{X}_{p,i}^{AC}$ and the future control sequence $\mathbb{X}_{\Delta,i}^{AC}$ presented in (6) and (7), respectively. Furthermore, the predicted vector $\mathbb{X}_{p,i}^{AC}$ is shared through the communication network.

$$J_{ac,i}(t_n) = \sum_{k=1}^{N_y} \lambda_{1i} (\bar{\omega}_i(t_{n+k}) - \omega_0)^2 + \sum_{k=1}^{N_u} \lambda_{2i} (\Delta\omega_{s,i}(t_{n+k-1}))^2 \\ + \sum_{j \in \mathbb{N}_{ac}} \sum_{k=1}^{N_y} \lambda_{3i} a_{ij}(t_n) \left(\frac{P_i(t_{n+k})}{P_{i \max}(t_n)} - \frac{P_j(t_{n+k-\hat{\tau}_{ij}})}{P_{j \max}(t_n)} \right)^2 \\ + \sum_{k=1}^{N_y} \lambda_{4i} (\bar{V}_{ac,i}(t_{n+k}) - V_{ac0})^2 + \sum_{k=1}^{N_u} \lambda_{5i} (\Delta V_{acs,i}(t_{n+k-1}))^2 \\ + \sum_{j \in \mathbb{N}_{ac}} \sum_{k=1}^{N_y} \lambda_{6i} a_{ij}(t_n) \left(\frac{Q_i(t_{n+k})}{|S_{i \max}|} - \frac{Q_j(t_{n+k-\hat{\tau}_{ij}})}{|S_{j \max}|} \right)^2 \quad (5)$$

$$\mathbb{X}_{p,i}^{AC} = \{\bar{\omega}_i(t_{n+k}), \omega_i(t_{n+k}), \delta\theta_i(t_{n+k}), P_i(t_{n+k}), \bar{V}_{ac,i}(t_{n+k}) \\ V_{ac,i}(t_{n+k}), Q_i(t_{n+k})\}_{k=1}^{N_y} \quad (6)$$

$$\mathbb{X}_{\Delta,i}^{AC} = \{\Delta\omega_{s,i}(t_{n+k-1}), \Delta V_{acs,i}(t_{n+k})\}_{k=1}^{N_u} \quad (7)$$

B. DMPC for DC sub-microgrid

The model used for the DMPC design is given by (8). The droop equation (8a) presents the relationship between the DGs' output voltage ($V_{dc,i}$), the active power transferred to the MG (P_i) computed by (8b), and the secondary control action ($V_{dcs,i}$). $M_{dc,i}$ is the droop slope, $G_i = 1/R_i$ and, $i \in \mathbb{N}_{dc}$. Note that (8) does not require information from other MG nodes to compute the power transfer; therefore, a model of the entire MG electrical is not required.

$$V_{dc,i}(t) = V_{dc0} + M_{dc,i} P_i(t) + V_{dcs,i}(t) \quad (8a)$$

$$P_i(t) = V_{dc,i}(t) \cdot I_{dc,i}(t) = G_i V_{dc,i}(t) (V_{dc,i}(t) - \hat{V}_{dc,i}^R(t)) \quad (8b)$$

In this case, $\hat{V}_{dc,i}^R$, defined by (9), is an estimation of the voltage after the coupling resistance R_i and is computed using Ohm's law. The proposed predictive control scheme for the DC-DGs of the DC sub-MG is shown in Fig. 3.

$$\hat{V}_{dc,i}^R = V_{dc,i} - I_{dc,i} R_i \quad (9)$$

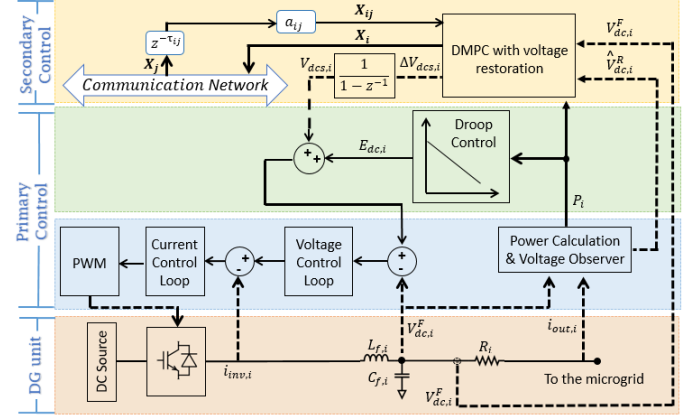


Fig. 3. DMPC_i Diagram for the DC DGs on the DC sub-MG.

The prediction models used for the proposed DMPC are based on (8). The discrete-time equations (10) are used as equality constraints to predict voltage and power trajectories over the prediction horizon N_y . Furthermore, the incremental operator is applied in (8a). Hence, the optimization problem is expressed as the control action variation ($\Delta V_{dcs,i}$). The measured/estimated point $\{V_{dc,i}(t_n), \hat{V}_{dc,i}^R(t_n), P_i(t_n)\}$ is used to linearize (8b). A local approximation of the MG average voltage is stated in equation (10c) which depends on the communication terms $a_{ij}(t_n)$ and the estimated delay ($\hat{\tau}_{ij}$), defined as one sample period at the secondary level. The terminal constraint (10d) guarantees the convergence of the DMPC to the DC nominal voltage at the end of the prediction horizon N_y [25].

$$V_{dc,i}(t_{n+k}) = V_{dc,i}(t_{n+k-1}) + M_{dc,i} [P_i(t_{n+k}) - P_i(t_{n+k-1})] \\ + \Delta V_{dcs,i}(t_{n+k-1}) \quad (10a)$$

$$P_i(t_{n+k}) = P_i(t_n) + [V_{dc,i}(t_{n+k}) - V_{dc,i}(t_n)] G_i [2V_{dc,i}(t_n) - \hat{V}_{dc,i}^R(t_n)] \quad (10b)$$

$$\bar{V}_{dc,i}(t_{n+k}) = \frac{V_{dc,i}(t_{n+k}) + \sum_{j \in \mathbb{N}_{dc}} a_{ij}(t_n) V_{dc,j}(t_{n+k-\hat{\tau}_{ij}})}{1 + \sum_{j \in \mathbb{N}_{dc}} a_{ij}(t_n)} \quad (10c)$$

$$\bar{V}_{dc,i}(t_{n+k}) = V_{dc0} \quad (10d)$$

Additionally, inequality constraints to limit the DG_i's output voltage (11a), active power rating (11b) and the rate of change of the control action (11c) are included to bound the solution space and improve the transient response of the controller.

$$V_{dc,min} \leq V_{dc,i}(t_{n+k}) \leq V_{dc,max} \quad (11a)$$

$a_{il}(t_n)$, $a_{jl}(t_n)$ and $a_{ILC,lj}(t_n)$, and the estimated delays ($\hat{\tau}_{il}$), ($\hat{\tau}_{jl}$) and ($\hat{\tau}_{lj}$).

$$\begin{aligned}
 J_{ILC,l}(t_n) &= \sum_{k=1}^{N_u} \lambda_{1l} (\Delta P_{ILC,l}(t_{n+k-1}))^2 \\
 &+ \sum_{i \in \mathbb{N}_{ac}} \sum_{j \in \mathbb{N}_{dc}} \sum_{k=1}^{N_y} \lambda_{2i} a_{il}(t_n) a_{jl}(t_n) \left(\frac{P_i(t_{n+k-\hat{\tau}_{il}})}{P_{i \max}} - \frac{P_j(t_{n+k-\hat{\tau}_{jl}})}{P_{j \max}} \right)^2 \\
 &+ \sum_{j \in \mathbb{N}_{ILC}} \sum_{k=1}^{N_y} \lambda_{3l} a_{ILC,lj}(t_n) \left(\frac{P_{ILC,l}(t_{n+k})}{P_{ILC,l \max}} - \frac{P_{ILC,j}(t_{n+k-\hat{\tau}_{lj}})}{P_{ILC,j \max}} \right)^2
 \end{aligned} \quad (20)$$

In this case, the consensus is carried out among the DGs with a direct communication link with the ILC_{*l*}, represented by the adjacency terms a_{il} and a_{jl} for AC and DC DGs, respectively. Although a full-meshed network could be considered to connect all devices in the MG, equations (5), (12) and (20) are defined considering a segmented network. It means that AC and DC DGs share information only among their pairs using dedicated networks, and at least one AC and one DC DG are connected to each ILC in the MG. This structure satisfies the connected-graph principle required to achieve a global consensus [26], while the total traffic through the communication network and its collateral issues are reduced [27].

Then, from (16)-(19) and (20), it is possible to derive a canonical QP problem to be deployed in each ILC secondary controller. The optimization output is composed of the predicted vector $\mathbb{X}_{p,l}^{ILC}$ and the future control sequence $\mathbb{X}_{\Delta,l}^{ILC}$ presented in (21) and (22), respectively.

$$\mathbb{X}_{p,l}^{ILC} = \{P_i(t_{n+k}), P_j(t_{n+k})\}_{k=1}^{N_y} \forall i \in \mathbb{N}_{ac} \ \& \ \forall j \in \mathbb{N}_{dc} \quad (21)$$

$$\mathbb{X}_{\Delta,l}^{ILC} = \{\Delta P_{ILC,l}(t_{n+k-1})\}_{k=1}^{N_u} \quad (22)$$

To sum up, the proposed controllers for AC DGs, DC DGs, and ILCs are based on local electrical models and information received from communicated neighbors. Both of them updated every sampling period t_n . Therefore, the proposed scheme tolerates changes in the electrical and communication networks, allowing the disconnection and reconnection of the DGs from/to the microgrid. This plug-and-play capability has been shown for this type of controller in [7] and [17]. Note that, as mentioned earlier, at least one AC DG and one DC DG must communicate with the ILC to achieve the global active power consensus (all the DGs share active power according to their nominal power capacity).

It is noted that the computational complexity of the method only depends on the prediction horizon (N_y). In fact, the number of variables and constraints in the optimization of each DG grows linearly with N_y . Since the optimization for each DG is the same and they are performed in parallel, the complexity for the entire optimization is driven by the linear increase in number of variables and constraints with the prediction horizon.

IV. EXPERIMENTAL SETUP AND RESULTS

The experimental hybrid AC/DC MG's topology used to validate the proposed control strategy is shown in Fig. 5. The

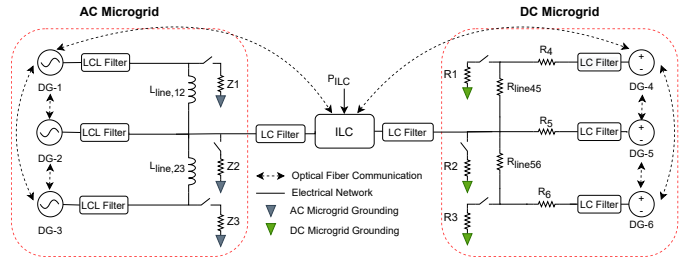


Fig. 5. Topology of the experimental hybrid AC/DC MG used for the validation of the proposed predictive control scheme.

TABLE I
HYBRID AC/DC MG PARAMETERS.

Parameter	Unit	Description	Value
T_{prim}	[s]	Primary level sampling time	$1/(16 \cdot 10^3)$
L_{fi}	[mH]	DG_i filter: inductor	0.85
C_{fi}	[μ F]	DG_i filter: capacitor	70
L_i	[mH]	$DG_{AC,i}$ coupling inductance	2.5
L_{line12}, L_{line23}	[mH]	AC-MG line inductor	2.5, 2.5
R_i	[Ω]	$DG_{DC,i}$ coupling resistor	0.67, 0.94, 0.47
R_{line45}, R_{line56}	[Ω]	DC-MG line resistance	0.78, 0.5
Z_1, Z_2, Z_3	[kW]	AC-MG loads	1.02, 1.50, 0.64
R_1, R_2, R_3	[kW]	DC-MG loads	1.54, 1.03, 1.54
S_1, S_2, S_3	[kW]	$DG_{AC}: S_{MAX}$	1.5, 1.5, 1.0
P_4, P_5, P_6	[kW]	$DG_{DC}: P_{MAX}$	2.0, 1.5, 1.5
$P_{ILC,1}, P_{ILC,2}$	[kW]	ILC: $P_{ILC,MAX}$	2.0, 10
ω_0	[$\frac{rad}{s}$]	AC-MG nominal frequency	314.159
V_{ac0}	[V]	AC-MG nominal voltage	150
V_{dc0}	[V]	DC-MG nominal voltage	130

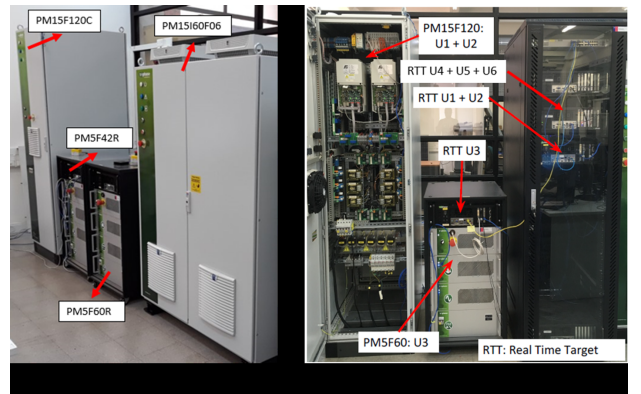


Fig. 6. Experimental hybrid AC/DC MG based on Triphase power converters. a) Triphase units. b) Real time computers.

TABLE II
DROOP SLOPES FOR THE PRIMARY CONTROL LOOP OF THE HYBRID AC/DC-MG.

Parameters	Unit	Droop slop	DG_1	DG_2	DG_3
$M_{p\omega}$	[rad/sW]	P- ω	$-3.3 \cdot 10^{-4}$	$-3.3 \cdot 10^{-4}$	$-5 \cdot 10^{-4}$
M_{qv}	[V/VAr]	Q-V	$-6.6 \cdot 10^{-3}$	$-6.6 \cdot 10^{-3}$	$-9.9 \cdot 10^{-3}$
			DG_4	DG_5	DG_6
M_{pv}	[V/W]	P-V	$-2.5 \cdot 10^{-3}$	$-3.3 \cdot 10^{-3}$	$-3.3 \cdot 10^{-3}$

experimental testbed is composed of two sub-MGs: one AC sub-MG and one DC sub-MG. Both sub-MGs are composed of three DGs. Note in Fig. 5 that an LCL output filter is used in each AC-DG unit. This approach allows the setting of the line impedances predominantly inductive (by a proper LCL design); thus, $P-\omega$ and $Q-V$ droop controllers are decoupled from each other [28]–[30]. Also, impedances Z_1 , Z_2 and Z_3

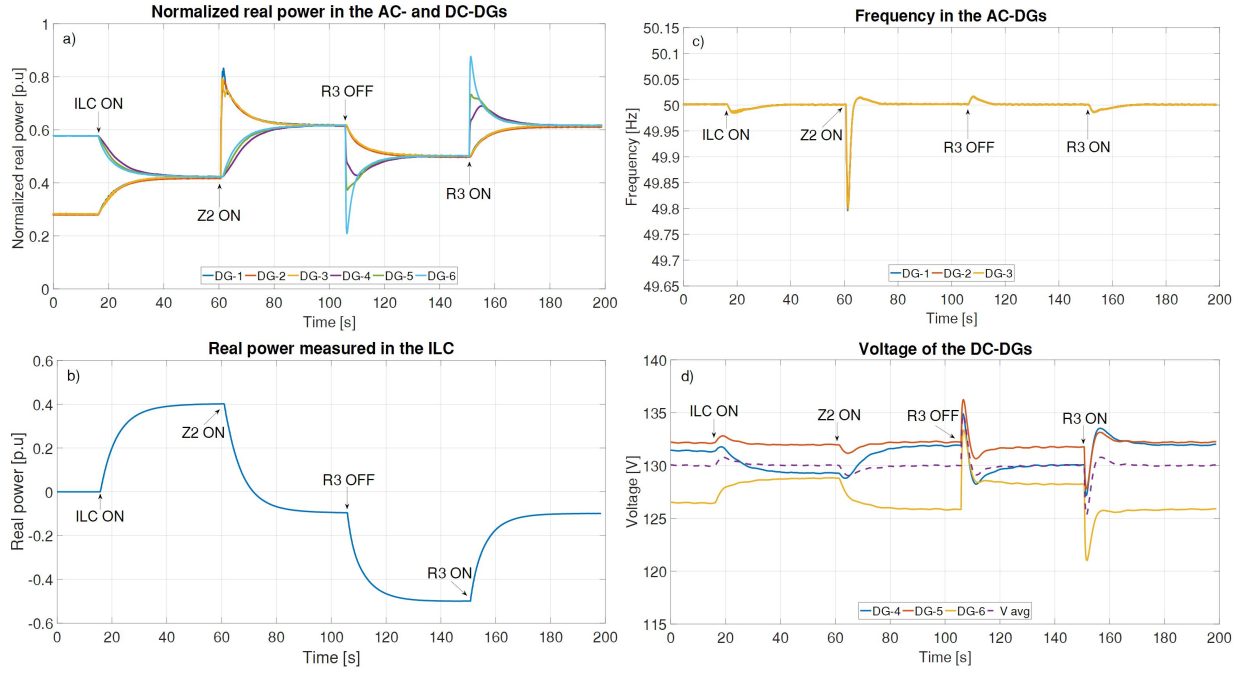


Fig. 7. Variables of the hybrid AC/DC MG under Scenario #1. a) Active power generated by AC-DGs and DC-DGs, in p.u. b) Active power transferred by the ILC. c) Frequency of the AC-DGs. d) DC-Voltage of the DC-DGs. DG-1 to DG-3 are AC-DGs and DG-4 to DG-6 are DC-DGs.

TABLE III
SECONDARY CONTROLLERS TUNING PARAMETERS.

Parameter	Unit	Description	Value
T_{sec}	[s]	Secondary controller sampling time	0.1
$\tilde{\tau}_{ij}$	[s]	Estimated communication delay	0.1
N_y	-	Prediction horizon	5
N_u	-	Control horizon	5
λ_{1i}	$[s/rad]^2$	Weighting factor for average frequency error	$2 \cdot 10^3$
λ_{2i}	$[s/rad]^2$	Weighting factor for frequency regulation	$9 \cdot 10^3$
λ_{3i}	$[VA/W]^2$	Weighting factor for active power consensus in ac-MG	$2 \cdot 10^2$
λ_{4i}	$[1/V]^2$	Weighting factor for average voltage error in ac-MG	$2 \cdot 10^3$
λ_{5i}	$[1/V]^2$	Weighting factor for voltage regulation in ac-MG	$9 \cdot 10^3$
λ_{6i}	$[VA/VAR]^2$	Weighting factor for reactive power consensus in ac-MG	$2 \cdot 10^2$
λ_{1i}	$[1/V]^2$	Weighting factor for average dc-voltage error	50
λ_{2i}	$[1/V]^2$	Weighting factor for dc-voltage regulation	55
λ_{3i}	-	Weighting factor for power consensus in dc-MG	$1.8 \cdot 10^4$
λ_{1l}	$[1/W]^2$	Weighting factor for ILC control action (ΔP_{ILC})	0.5
λ_{2l}	-	Weighting factor active power consensus in the ILC	$8 \cdot 10^5$

(see Fig. 5) are considered as resistive loads. The DC-DG units also feed resistive loads and coupling resistors for the DMPC model and series resistors for the transmission line emulation. Finally, both sub-MGs are connected using an ILC, which allows a bidirectional power transfer between both sub-MGs. The MG electrical parameters are compiled in Table I.

The communication network implemented in this experimental MG uses fibre optical cables and is represented in Fig. 5 (see dashed lines). It considers full communication inside each sub-MG, i.e., each AC-DG communicates with all the other AC-DGs, and each DC-DG communicates with

all the other DC-DGs. Additionally, one AC-DG and one DC-DG communicate with the ILC. Note that this is the worst possible communication scenario, as only one DG on each side is communicated directly to the ILC [26]. The MG testbed is based on Triphase[®] units, as shown in Fig. 6 and developed using Matlab/Simulink[®]. More details about the experimental hybrid AC/DC MG are presented in [31].

A heuristic methodology was applied for tuning the weighting factors of the DMPCs. Firstly, the control action variation is tuned to produce a soft action for the controller. Secondly, for the AC-MG controllers, a compromise is defined between frequency regulation and active power consensus. For the DC-MG controllers, the compromise is defined between the average DC-voltage regulation and the power consensus. In both cases, the controllers are tuned to reach nominal values of the frequency and the average DC-voltage, respectively, while the DGs achieve power consensus. The parameters for primary and secondary controllers are shown in Table II and Table III.

The following two scenarios are presented to validate experimentally the proposed DMPC scheme's performance: load impacts and communication network delays. The former scenario is considered the base case. To reduce traffic on the communication network, for the experimental validation the AC voltage regulation and the reactive power sharing are controlled using the DAPI-based method reported in [8].

A. Scenario #1 (Base case) - Load impacts

In this test, four resistive load impacts are applied on both sides of the hybrid AC/DC MG in order to validate: (i) the frequency and voltage regulation using the proposed DMPC scheme, (ii) the active power consensus between all the DGs

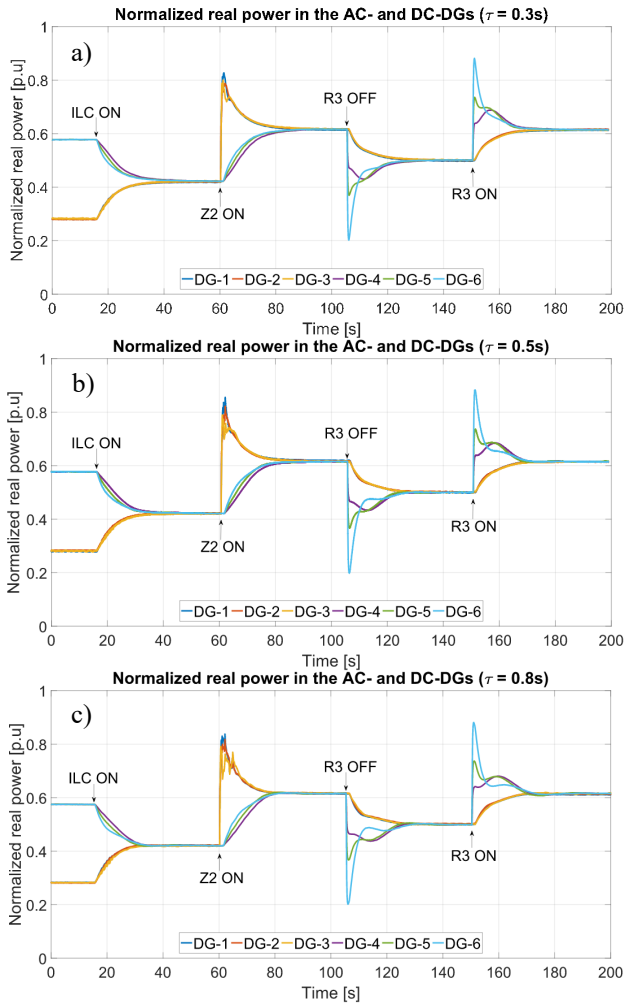


Fig. 8. Communication delays experimental test. Active power generated by AC-DGs and DC-DGs, in p.u., when applying a delay equal to: a) $\tau = 0.3s$, b) $\tau = 0.5s$, and c) $\tau = 0.8s$. DG-1 to DG-3 are AC-DGs and DG-4 to DG-6 are DC-DGs.

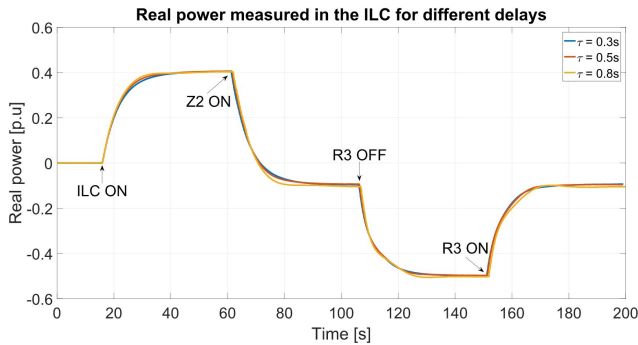


Fig. 9. Active power transferred by the ILC considering different delays in the communication network.

in the MG, and (iii) the bidirectional power transfer capability of the ILC.

At $t = 0s$, the hybrid MG starts operating with the primary control loops and the secondary predictive controllers on the AC sub-MG and the DC sub-MG enabled, whereas the DMPC for the ILC is disabled. The power load on the AC sub-MG

is equal to $1.02kW$ (only Z_1 is connected), while the power load on the DC sub-MG is equal to $3.08kW$ (R_1 and R_3 are connected). As the ILC's predictive controller is disabled, the power consensus is achieved separately by the AC-DGs and by the DC-DGs on their respective sides (see Fig. 7.a before $t = 15s$), and the frequency and average DC voltage are kept at their nominal values, as shown in Fig. 7.c and Fig. 7.d, respectively.

The ILC is connected at $t = 15s$. Thus, the power sharing between both sub-MGs starts. The loading condition of the DC sub-MG is higher than that of the AC sub-MG (see Fig. 7.a). Therefore, the power transferred through the ILC is positive, and the power moves from the AC sub-MG to the DC sub-MG, as depicted in Fig. 7.b after $t = 15s$ and onwards. The proposed DMPC set of controllers maintains an adequate regulation of the frequency and the average dc-voltage. At the same time, the power consensus is achieved between the AC-DGs and the DC-DGs, as shown in Fig. 7.c and Fig. 7.d.

The load on the AC sub-MG is increased from $1.02kW$ to $2.52kW$ at $t = 60s$. As the loading in the AC sub-MG increases, the power transferred through the ILC decreases and becomes negative as shown in Fig. 7.b, which means that now the power is transferred from the DC sub-MG to the AC sub-MG. After $20s$ ($t = 80s$), all the DGs contribute active power in the same proportion; thus, the power consensus is achieved as depicted in Fig. 7.a, while both the frequency and the average DC-voltage are regulated correctly (see Fig. 7.c and Fig. 7.d). The settling time for AC and DC power consensus is governed by the ILC dynamics, which uses a constraint over the rate of change of its control action ΔP_{ILC_i} . Furthermore, as only one DG controller of each sub-MG is connected to the ILC controller (see Fig. 5), the ILC controller has a slow dynamic response. This is because the performance of the DMPC for the ILC also depends on the dynamic of the adjacency matrix A , which was selected as the worst possible communication scenario with only one direct communication channel from each side to the ILC [26].

A DC-load equal to $1.54kW$ (R_1) is disconnected and, then, reconnected to bus 3 on the DC sub-MG at $t = 105s$ and $t = 150s$, respectively. As long as the loading on the DC sub-MG is reduced, i.e., load R_3 is disconnected, the power transferred from the DC sub-MG to the AC sub-MG increases, as shown in Fig. 7.b. The regulation performance of the frequency on the AC sub-MG and the DC-voltage on the DC sub-MG is correct during all the tests, as shown in Fig. 7.c and Fig. 7.d, respectively.

As expected, the sub-MG that is affected the most for a certain load impact corresponds to the one where the load is connected. For example, at $t = 60s$, the AC-load impact affects more the frequency as depicted in Fig. 7.c. However, the average DC-voltage is also affected due to the relation of both sub-MGs through the ILC, as shown in Fig. 7.d.

B. Scenario #2 - Communication delays

In the test scenario #2, issues in the fibre optical communication network of the experimental setup of Fig. 5 are addressed. Specifically, the robustness of the proposed control

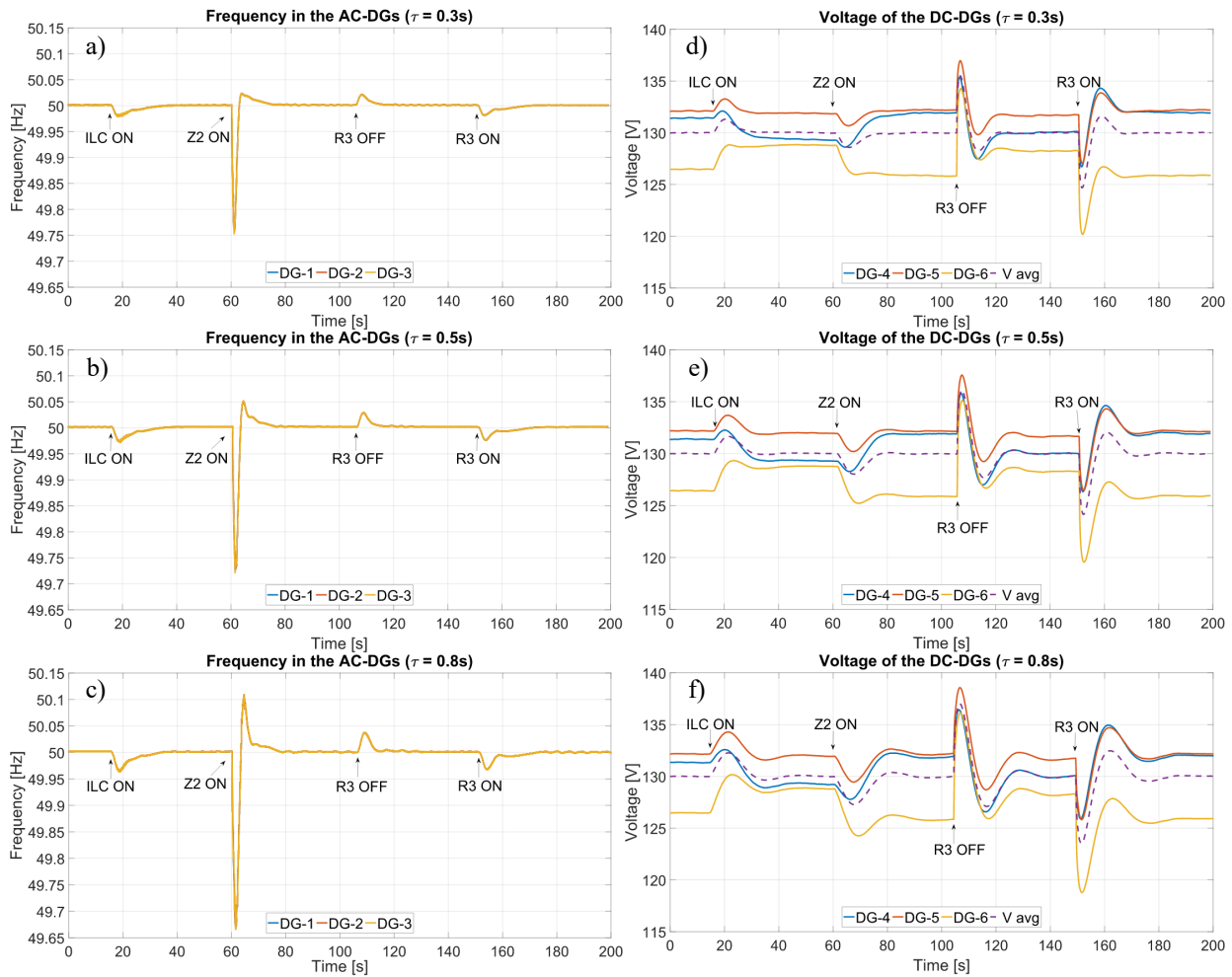


Fig. 10. Communication delays experimental test. Frequency of the AC-DGs, in hertz, when applying a delay equal to: a) $\tau = 0.3s$, b) $\tau = 0.5s$, and c) $\tau = 0.8s$. DC-Voltage of the DC-DGs, in volts, when applying a delay equal to: d) $\tau = 0.3s$, e) $\tau = 0.5s$, and f) $\tau = 0.8s$. DG-1 to DG-3 are AC-DGs and DG-4 to DG-6 are DC-DGs.

strategy against transport delays in the communication network is analyzed. The delays considered in this test are $\tau = 0.3s$, $0.5s$ and $0.8s$, while the estimated delay $\hat{\tau}_{ij}$ is kept constant as one sampling period. Note that the latter two time delays used to evaluate the proposal's performance can be considered as medium and large delays (see [16], [32]).

For this test, the operating point is the one described in the base case (section IV-A). Furthermore, the load impacts applied to each test are the same as the ones described in the base case. From the results obtained in this test, it is seen that power-sharing between the DGs is achieved in steady state, despite the different delays applied to the communication network (see power generated by the AC-DGs and the DC-DGs in Fig. 8.a, Fig. 8.b and Fig. 8.c, respectively for the different delays applied). A small difference can be seen when analyzing the transient response of the power generated by the DGs against the delays: as the delay increases, the oscillation also increases. Although the transient response is different for each sub-case analyzed, the power transferred by the ILC is slightly affected as shown in Fig. 9, and the control objectives are achieved when the system reaches steady state operation. Therefore, the DMPC scheme is resilient to what is considered

a large communication delay at the secondary level.

The frequency and the average DC-voltage are more affected as the communication delay increases, as shown in Fig. 10. From the figures, it is clear that, when the delay grows, the transient response becomes more oscillatory. Furthermore, the frequency and the voltage deviations (during the transient response) are larger when loads are connected and the delay is higher. However, the DMPC scheme still achieves its control objectives and both the frequency and the average DC-voltage are restored to their nominal values in steady state.

The proposed DMPC can handle the communication delay issues due to its rolling horizon scheme, which updates the control actions at every sampling time and compensates the effects produced by delays. It is worth noting that, the effects produced by delays depend on the prediction horizon, control horizon, sampling time, and estimated delay $\hat{\tau}_{ij}$.

V. SIMULATION RESULTS

This section complements the validation of the proposed DMPC control scheme using simulation studies. In this section, the plug-and-play capability and the operation with multiple ILCs are evaluated in a MG simulator. For this purpose,

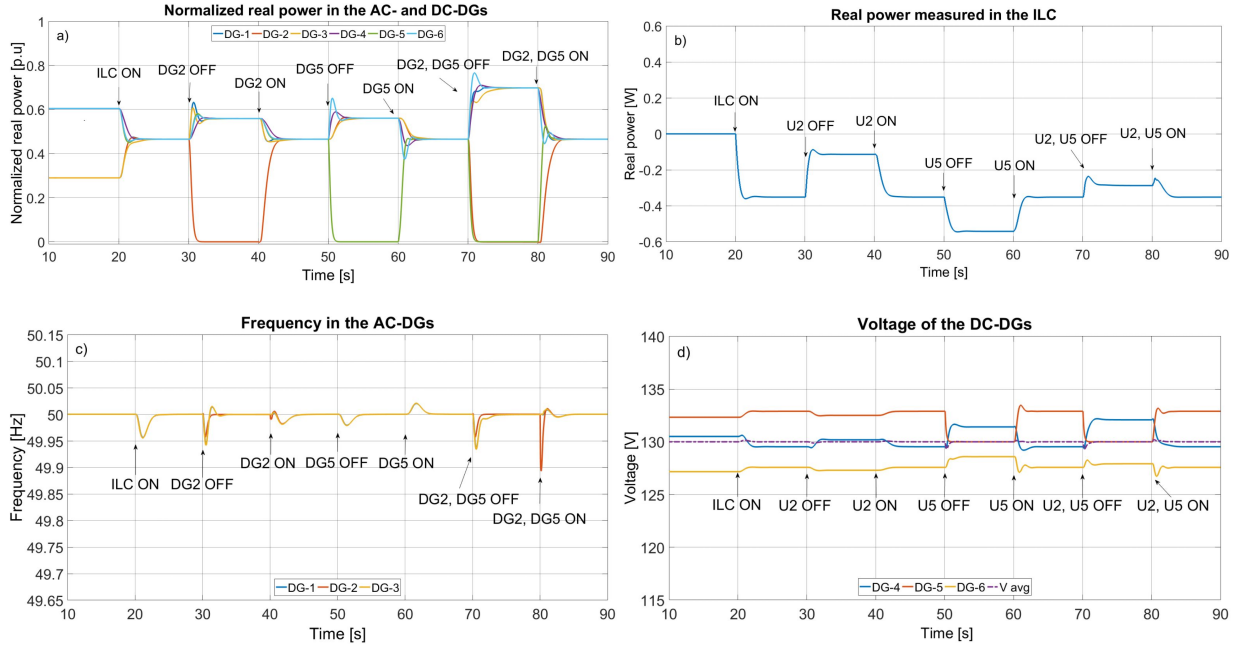


Fig. 11. Variables of the hybrid AC/DC MG for Plug-and-Play test. a) Active power generated by AC-DGs and DC-DGs, in p.u. b) Active power transferred by the ILC. c) Frequency of the AC-DGs. d) DC-Voltage of the DC-DGs. DG-1 to DG-3 are AC-DGs and DG-4 to DG-6 are DC-DGs.

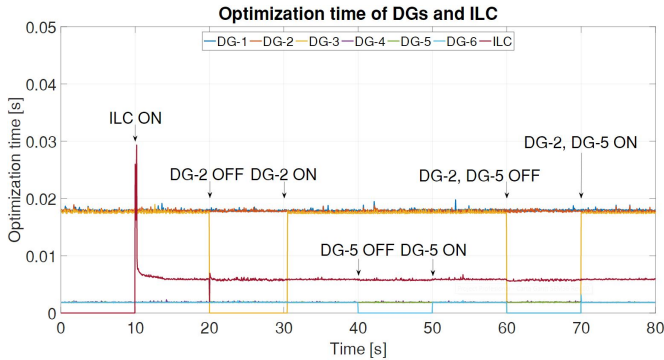


Fig. 12. Optimization time for the plug-and-play test

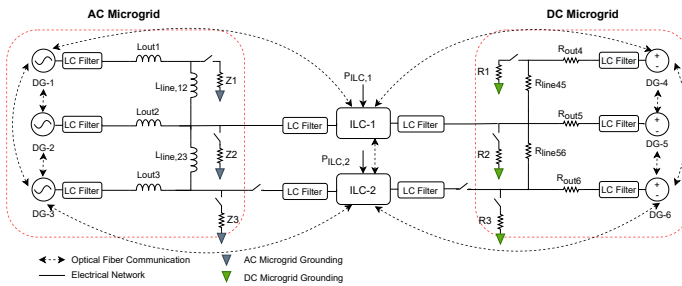


Fig. 13. Topology of the simulated hybrid AC/DC MG with multiple ILCs.

an MG simulator is developed where the MG electrical model is built in the *Plecs Blockset*, and the primary and secondary controllers are implemented in the *MATLAB-Simulink* environment. This simulator faithfully represents the experimental setup because details such as inner current and voltage loops,

droop controllers, and output filters are modeled. The same electrical and control parameters of the experimental setup are replicated in the MG simulator, as illustrated in Table I and Table III, respectively.

A. Plug-and-Play capability

In this test, a DG on each side of the hybrid AC/DC MG is disconnected and then reconnected from both the MG and the communication network. The load condition is established by Z_1 on the AC sub-MG and by R_1 and R_3 on the DC sub-MG. The load condition is kept constant during the whole test. The test starts with the predictive controllers for the AC and DC sub-MGs enabled, but the ILC predictive controller is disabled. At $t = 20s$ the ILC predictive controller is enabled. The results are presented in Fig. 11. It is observed that when the ILC predictive controller is enabled ($t = 20s$), the whole active power consensus on the hybrid MG is achieved (see Fig. 11.a), and the frequency and voltage present slight deviations that are immediately corrected by the controllers on each sub-MG (see Fig. 11.c and Fig. 11.d).

Then at $t = 30s$ and $t = 40s$ the AC-DG₂ is disconnected and reconnected (on the AC sub-MG), respectively. When DG₂ is disconnected ($t = 30s$), the remaining DGs update their received information, i.e., the adjacency matrix A is modified, and with it the consensus and average terms in all the operating predictive controllers. Furthermore, because of the disconnection of DG₂ on the AC sub-MG, the power transferred through the ILC is reduced (see Fig. 11.b). Note that when a DG is disconnected, its predictive controller is disabled, and it will only be enabled again when the DG unit is reconnected.

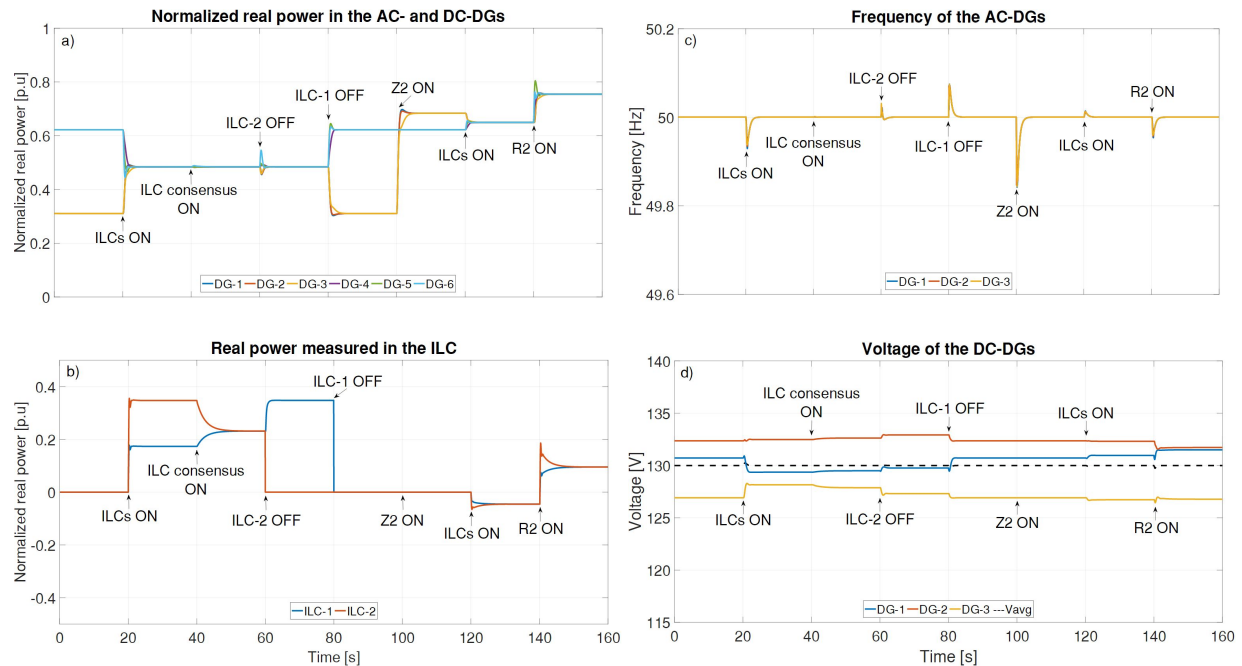


Fig. 14. Variables of the hybrid AC/DC MG for multiple ILCs operation. a) Active power generated by AC-DGs and DC-DGs, in p.u. b) Active power transferred by the ILC. c) Frequency of the AC-DGs. d) DC-Voltage of the DC-DGs. DG-1 to DG-3 are AC-DGs and DG-4 to DG-6 are DC-DGs.

In a similar way, at $t = 50s$ and $t = 60s$ DC-DG₅ is disconnected and reconnected (on the DC sub-MG), respectively. As a result of this event, the AC sub-MG compensates for the deficit, increasing the power transferred through the ILC (see Fig. 11.b). Finally, the plug-and-play capability is further verified by disconnecting and reconnecting both DGs simultaneously at $t = 70s$ and $t = 80s$, respectively. Note that even when two DGs are disconnected ($t = 70s$) or reconnected ($t = 80s$) at the same time, the MG continues operating normally, and the predictive controllers recognize these events to provide the necessary control action sequences and fulfill all the control objectives. These results verify that the proposed set of controllers can handle the disconnection and reconnection of DGs and show that the use of hybrid MGs with an ILC can cope with the deficit in the load condition that a DG failure on either side can cause.

The time to find a solution for the DMPC scheme is presented in Fig. 12. All predictive controllers of the AC-DGs sub-MG find a solution in around 0.02 seconds, while the predictive controllers of the DC-DGs and ILC reach a solution within 0.01 seconds. Note that the aforementioned times are well below the sample time (0.1 seconds). It should be noted that due to the distributed structure of the predictive scheme, the number of optimization variables is fixed (see Equations (6) and (7) for the AC-DGs, Equations (13) and (14) for the AC-DGs, Equations (21) and (22) for the ILCs). Fig. 12 shows that the time required to obtain a solution does not vary when DGs are disconnected or connected. These tests were performed on a 9th generation Intel Core i7 3.6GHz computer with 32GB of RAM. This shows that the complexity of the method is such that it can be effectively applied in real time with the currently available hardware.

B. Operation with multiple ILCs

In this section, the performance of the proposed controller when there are two ILCs in the hybrid MG is evaluated. For this purpose, a second ILC is connected, as shown in Fig. 13. Note that the new ILC (ILC-2) has communication with both AC-side and DC-side, and with the other ILC (ILC-1) (see dashed lines in Fig. 13). The test starts with the predictive controllers for the AC and DC sub-MGs enabled, but the predictive controllers of the ILCs are disabled. The results are presented in Fig. 14. At $t = 20s$ the predictive controllers of the ILCs are enabled, but without considering the third term of (20) (consensus between ILCs). It is observed that the active power consensus between the AC and DC sub-MGs is achieved (see Fig. 14.a), and the frequency regulation on the AC sub-MG (see Fig. 14.c) and the DC voltage regulation (see Fig. 14.d) are not affected. However, as there is no active power consensus between ILCs, the active power is transferred through the ILCs without considering the ILCs' power rating (see Fig. 14.b) between $t = 20s$ and $t = 40s$, which could lead to overloading the ILC with lower power rating (ILC-2).

At $t = 40s$ the power consensus between ILCs is enabled, as a result both ILCs contribute to the power transfer proportionally to their power rating (see Fig. 14.b between $t = 40s$ and $t = 60s$), reducing the operational burden in ILC-2. Then, at $t = 60s$ and $t = 80s$ ILC-2 and ILC-1 are disconnected, respectively. It is observed that when one ILC is disconnected, the other transfer the whole active power (see Fig. 14.b) between $t = 60s$ and $t = 80s$). Furthermore, when both ILCs are disconnected (see Fig. 14.b) between $t = 80s$ and $t = 100s$), there is no longer power transfer between sub-MGs, and they operate independently. Nevertheless, they maintain power consensus between the DGs that belong to

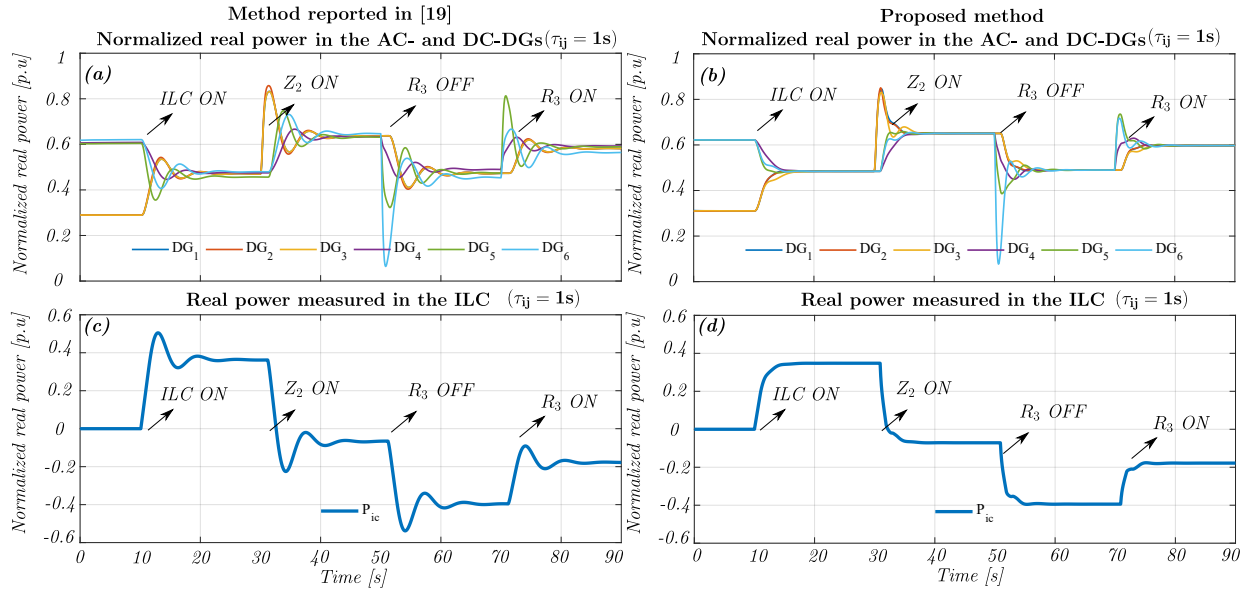


Fig. 15. Comparison between the proposed DMPC scheme and the method reported in [19]. a)-b) Active power generated by AC-DGs and DC-DGs, in p.u for the two methods compared. c)-d) Active power transferred by the ILC for the two methods compared.

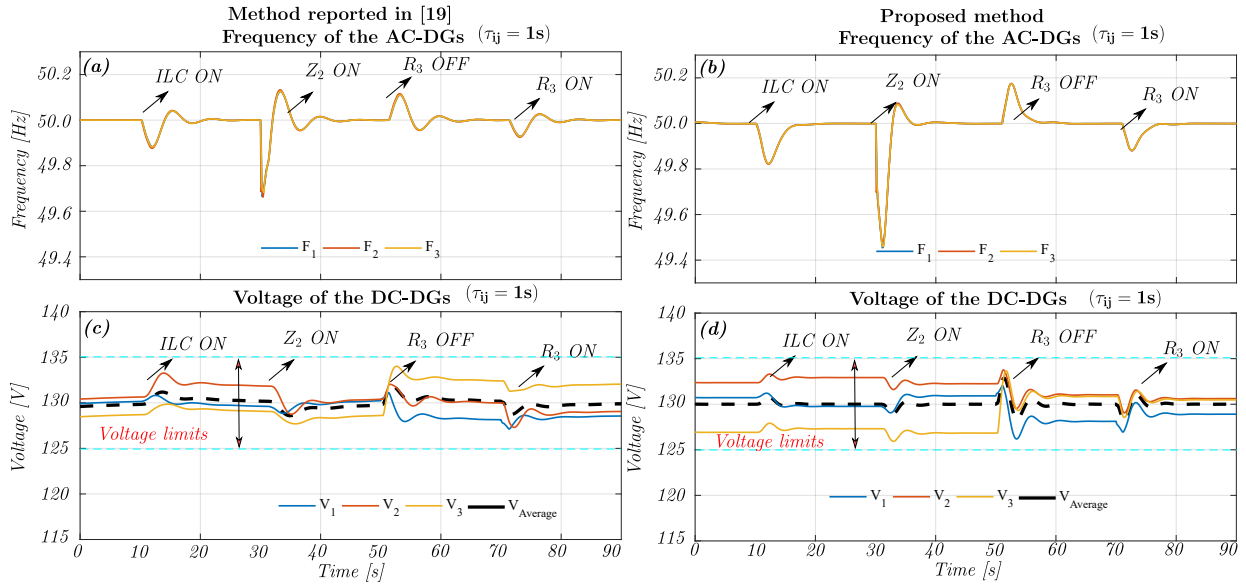


Fig. 16. Comparison between the proposed DMPC scheme and the method reported in [19]. a)-b) Frequency of the AC-DGs for the two methods compared. c)-d) DC-Voltage of the DC-DGs for the two methods compared. DG-1 to DG-3 are AC-DGs and DG-4 to DG-6 are DC-DGs. The dashed cyan lines represent the voltage limits.

each sub-MG, as shown in Fig. 14.a between $t = 80s$ and $t = 100s$.

At $t = 100s$, a load on the AC sub-MG is connected, but as there is no connection with the DC sub-MG (both ILCs disabled), only the AC-DGs increase their power contribution to a 70% approximately. At $t = 120s$, both ILCs are enabled, and as expected, all the objectives are achieved instantaneously. Finally, at $t = 140s$, a load on the DC sub-MG is connected. These results verify that the proposed set of controllers can manage multiple ILCs. Furthermore, the proposed technique is fully compatible with the plug-and-play concept, allowing the disconnection and reconnection of not only DGs on both

sub-MGs but also the disconnection and reconnection of ILCs.

VI. COMPARISON WITH A DAPI-BASED CONTROLLER

In this section, a comparison via simulation between the proposed DMPC and the DAPI-based controller proposed in [19] is provided, which is a DAPI-based controller. This comparison is suitable because both control techniques include regulation and consensus objectives in a distributed fashion for hybrid MGs. Both schemes use an adjacency matrix to represent the communication topology. The work of [19] is based on the DAPI control scheme and, among its objectives, seeks frequency regulation, DC and AC voltage regulation, and

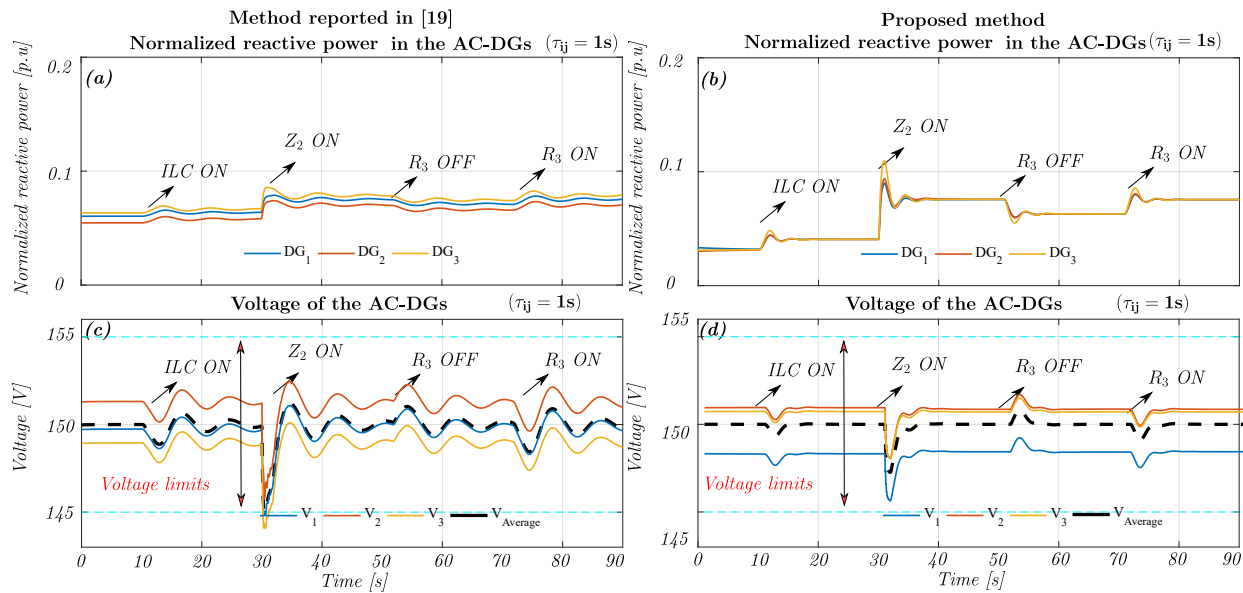


Fig. 17. Comparison between the proposed DMPC scheme and the method reported in [19]. a)-b) Reactive power generated by AC-DGs in p.u for the two methods compared. c)-d) AC-Voltage of the AC-DGs for the two methods compared. DG-1 to DG-3 are AC-DGs. The dashed cyan lines represent the voltage limits.

active and reactive power sharing. The MG simulator depicted in Fig. 6 is used for comparison purposes.

In this comparison, communication delays were studied. This scenario was selected because robustness under delays is essential for distributed controllers. In this test, a constant delay of one second ($\tau_{ij} = 1s$) is applied to the entire communication network, and the performance of both strategies is evaluated. The results for [19] are presented on the left side of Fig. 15, Fig. 16 and Fig. 17, whereas the results the proposed DMPC are depicted on the right side of the aforementioned figures. It is observed that the technique reported in [19] is affected under large delays by presenting overshoots and oscillations in its behavior and increasing its settling time when the MG load condition changes. In contrast, the proposed DMPC is slightly affected in its transitory response. The DMPC reduces the overshoots and has a faster settling time. Furthermore, the consensus objectives are achieved regardless of the delay. This is because the DMPC possesses the rolling horizon property and delay estimation. The DMPC scheme corrects the control actions sequence [21], while the DAPI technique [19] does not possess a delay compensation property.

Note that the work of [19] neither achieves exact active power consensus nor achieves reactive power consensus (see Fig. 15.a, and Fig. 17.a). This is because this work tries to regulate all the output voltages of the DC-DGs and AC-DGs to nominal values. This creates a trade-off between DC voltage regulation and active power sharing and AC voltage regulation and reactive power sharing. Conversely, the proposed DMPC restores the average AC voltage and the average DC voltage to nominal values and achieves exact active and reactive power sharing, as shown in the right-hand side of Fig. 15, Fig. 16 and Fig. 17, respectively. Note that in the AC voltage comparison (see Fig. 17.c and Fig. 17.d) due to the voltage limit constraint,

Equation (4a), all the output voltages are within the desired limits (see the dashed cyan lines in Fig. 17.d), while the DAPI controller in an effort to improve reactive power sharing sacrifices AC voltage regulation (see the dashed cyan lines in Fig. 17.c). This result verifies that the proposed DMPC can tackle operational limits constraints within the formulation, while achieving multiple objectives with a reduced number of control actions. Conversely, in DAPI-based techniques, such as [19], [20], [33], only a saturation is used if a DG reaches an operational limit. Furthermore, on these approaches, if more objectives are added, more control actions are needed.

VII. CONCLUSIONS AND FINAL REMARKS

In this paper, a distributed model-based predictive control strategy for hybrid AC/DC MGs has been proposed. This strategy restores the nominal values of the frequency of the AC sub-MG and the average voltage on the DC sub-MG. Over the same time scale the proposed strategy achieves an active power consensus. The power-sharing between both the AC sub-MG and the DC sub-MG is achieved by transferring power through an interlinking converter, which allows a bidirectional power transfer. The proposed strategy considers a rolling horizon scheme, which can compensate for delays in the communication network. The better performance of the proposed strategy under communication delays, when compared with traditional DAPI-based controllers, is validated via simulation studies.

Experimental tests were carried out in a hybrid AC/DC MG, where the effectiveness of the proposed controller against load impacts was demonstrated. Furthermore, communication network issues, i.e. delays in the communication network and the plug-and-play capability were evaluated. The proposed distributed predictive control strategy presented a good performance in all the analyzed cases. Future research will be

focused on the stability analysis of the proposed distributed technique, the consideration of inductive and resistive line impedances in the DMPC formulation, and adding the ILC the capability to support the AC sub-MG in the reactive power sharing and AC voltage regulation.

REFERENCES

- [1] S. K. Sahoo, A. K. Sinha, and N. K. Kishore, "Control Techniques in AC, DC, and Hybrid AC–DC Microgrid: A Review," *IEEE J. Emerg. Sel. Top. Power Electron.*, vol. 6, no. 2, pp. 738–759, Jun. 2018.
- [2] F. Nejabatkhah and Y. W. Li, "Overview of Power Management Strategies of Hybrid AC/DC Microgrid," *IEEE Trans. Power Electron.*, vol. 30, no. 12, pp. 7072–7089, Dec. 2015.
- [3] G. S. Rawat and Sathans, "Survey on DC microgrid architecture, power quality issues and control strategies," in *2018 2nd Int. Conf. Inven. Syst. Control*, no. Icisc. IEEE, Jan. 2018, pp. 500–505.
- [4] D. Kumar, F. Zare, and A. Ghosh, "DC Microgrid Technology: System Architectures, AC Grid Interfaces, Grounding Schemes, Power Quality, Communication Networks, Applications, and Standardizations Aspects," *IEEE Access*, vol. 5, pp. 12230–12256, Jun. 2017.
- [5] IEEE Power and Energy Society, "IEEE Standard for the Specification of Microgrid Controllers IEEE Standard for the Specification of Microgrid Controllers," pp. 1–42, 2017.
- [6] Y. Han, H. Li, P. Shen, E. A. A. Coelho, and J. M. Guerrero, "Review of Active and Reactive Power Sharing Strategies in Hierarchical Controlled Microgrids," *IEEE Trans. Power Electron.*, vol. 32, no. 3, pp. 2427–2451, Mar. 2017.
- [7] J. S. Gomez, D. Saez, J. W. Simpson-Porco, and R. Cardenas, "Distributed Predictive Control for Frequency and Voltage Regulation in Microgrids," *IEEE Trans. Smart Grid*, vol. 11, no. 2, pp. 1319–1329, Mar. 2020.
- [8] J. W. Simpson-Porco, Q. Shafiee, F. Dorfler, J. C. Vasquez, J. M. Guerrero, and F. Bullo, "Secondary Frequency and Voltage Control of Islanded Microgrids via Distributed Averaging," *IEEE Trans. Ind. Electron.*, vol. 62, no. 11, pp. 7025–7038, Nov. 2015.
- [9] Y. Han, K. Zhang, H. Li, E. A. A. Coelho, and J. M. Guerrero, "MAS-Based Distributed Coordinated Control and Optimization in Microgrid and Microgrid Clusters: A Comprehensive Overview," *IEEE Trans. Power Electron.*, vol. 33, no. 8, pp. 6488–6508, Aug. 2018.
- [10] E. Espina, J. Llanos, C. Burgos-Mellado, R. Cardenas-Dobson, M. Martinez-Gomez, and D. Saez, "Distributed Control Strategies for Microgrids: An Overview," *IEEE Access*, vol. 8, pp. 193412–193448, oct 2020.
- [11] A. Gupta, S. Doolla, and K. Chatterjee, "Hybrid AC–DC Microgrid: Systematic Evaluation of Control Strategies," *IEEE Trans. Smart Grid*, vol. 9, no. 4, pp. 3830–3843, Jul. 2018.
- [12] Y. Xia, W. Wei, M. Yu, X. Wang, and Y. Peng, "Power Management for a Hybrid AC/DC Microgrid With Multiple Subgrids," *IEEE Trans. Power Electron.*, vol. 33, no. 4, pp. 3520–3533, Apr. 2018.
- [13] M. Hosseinzadeh and F. R. Salmasi, "Robust optimal power management system for a hybrid AC/DC micro-grid," *IEEE Trans. Sustain. Energy*, vol. 6, no. 3, pp. 675–687, Jul. 2015.
- [14] M. Manbachi and M. Ordóñez, "AMI-Based Energy Management for Islanded AC/DC Microgrids Utilizing Energy Conservation and Optimization," *IEEE Trans. Smart Grid*, vol. 10, no. 1, pp. 293–304, Jan. 2019.
- [15] P. Wang, X. Lu, X. Yang, W. Wang, and D. Xu, "An Improved Distributed Secondary Control Method for DC Microgrids With Enhanced Dynamic Current Sharing Performance," *IEEE Trans. Power Electron.*, vol. 31, no. 9, pp. 6658–6673, Sep. 2016.
- [16] J. Llanos, D. E. Olivares, J. W. Simpson-Porco, M. Kazerani, and D. Saez, "A novel distributed control strategy for optimal dispatch of isolated microgrids considering congestion," *IEEE Trans. Smart Grid*, vol. 10, no. 6, pp. 6595–6606, Nov. 2019.
- [17] A. Navas F., J. S. Gomez, J. Llanos, E. Rute, D. Saez, and M. Sumner, "Distributed Predictive Control Strategy for Frequency Restoration of Microgrids Considering Optimal Dispatch," *IEEE Trans. Smart Grid*, vol. 12, no. 4, pp. 2748–2759, Jul. 2021.
- [18] M. J. Rana and M. A. Abido, "Energy management in DC microgrid with energy storage and model predictive controlled AC–DC converter," *IET Gener. Transm. Distrib.*, vol. 11, no. 15, pp. 3694–3702, Oct. 2017.
- [19] E. Espina, R. Cardenas-Dobson, J. W. Simpson-Porco, D. Saez, and M. Kazerani, "A Consensus-Based Secondary Control Strategy for Hybrid AC/DC Microgrids with Experimental Validation," *IEEE Trans. Power Electron.*, vol. 36, no. 5, pp. 5971–5984, May 2021.
- [20] H. J. Yoo, T. T. Nguyen, and H. M. Kim, "Consensus-based distributed coordination control of hybrid AC/DC microgrids," *IEEE Trans. Sustain. Energy*, vol. 11, no. 2, pp. 629–639, Apr. 2020.
- [21] J. Hu, Y. Shan, J. M. Guerrero, A. Ioinovici, K. W. Chan, and J. Rodriguez, "Model predictive control of microgrids – An overview," *Renew. Energy Rev.*, vol. 136, p. 110422, Feb. 2021.
- [22] C. Ahumada, R. Cárdenas, D. Sáez, and J. M. Guerrero, "Secondary Control Strategies for Frequency Restoration in Islanded Microgrids With Consideration of Communication Delays," *IEEE Trans. Smart Grid*, vol. 7, no. 3, pp. 1430–1441, May 2016.
- [23] J. Solsona and A. Leon, "Design of reduced-order nonlinear observers for energy conversion applications," *IET Control Theory Appl.*, vol. 4, no. 5, pp. 724–734, May 2010.
- [24] C. Burgos-Mellado, A. Costabeber, M. Sumner, R. Cárdenas-Dobson, and D. Sáez, "Small-signal modelling and stability assessment of phase-locked loops in weak grids," *Energies*, vol. 12, no. 7, p. 1227, 2019.
- [25] E. F. Camacho and C. Bordons, "Constrained Model Predictive Control," in *Model Predict. Control*, 2nd ed., ser. Advanced Textbooks in Control and Signal Processing. London: Springer London, 2007, no. Dec., ch. 7, pp. 177–216.
- [26] F. Bullo, "Lectures on Network Systems," in *Lect. Netw. Syst.* Version 0.96, 2018, ch. 4, pp. 47–61, with contributions by J. Cortes, F. Dorfler, and S. Martinez.
- [27] Y.-B. Zhao, X.-M. Sun, J. Zhang, and P. Shi, "Networked Control Systems: The Communication Basics and Control Methodologies," *Math. Probl. Eng.*, vol. 2015, pp. 1–9, Jun. 2015.
- [28] M. Savaghebi, A. Jalilian, J. C. Vasquez, and J. M. Guerrero, "Autonomous voltage unbalance compensation in an islanded droop-controlled microgrid," *IEEE Trans. Ind. Electron.*, vol. 60, no. 4, pp. 1390–1402, Apr. 2012.
- [29] M. B. Said-Romdhane, M. W. Naouar, I. S. Belkhdja, and E. Monmasson, "An improved lcl filter design in order to ensure stability without damping and despite large grid impedance variations," *Energies*, vol. 10, no. 3, p. 336, Mar. 2017.
- [30] C. Burgos-Mellado, R. Cárdenas, D. Saez, A. Costabeber, and M. Sumner, "A control algorithm based on the conservative power theory for cooperative sharing of imbalances in four-wire systems," *IEEE Trans. Power Electron.*, vol. 34, no. 6, pp. 5325–5339, Jun. 2018.
- [31] E. Espina, C. Burgos-Mellado, J. S. Gomez, J. Llanos, E. Rute, M. Martinez, R. Cardenas, and D. Saez, "Experimental Hybrid AC / DC-Microgrid Prototype for Laboratory Research," in *2020 22st Eur. Conf. Power Electron. Appl. (EPE '20 ECCE Eur.*, IEEE, Ed., no. Sep., Lyon, 2020.
- [32] G. Chen and Z. Guo, "Distributed secondary and optimal active power sharing control for islanded microgrids with communication delays," *IEEE Trans. Smart Grid*, vol. 10, no. 2, pp. 2002–2014, Mar. 2017.
- [33] C. Burgos-Mellado, J. J. Llanos, R. Cárdenas, D. Sáez, D. E. Olivares, M. Sumner, and A. Costabeber, "Distributed control strategy based on a consensus algorithm and on the conservative power theory for imbalance and harmonic sharing in 4-wire microgrids," *IEEE Transactions on Smart Grid*, vol. 11, no. 2, pp. 1604–1619, Mar. 2020.



Erwin Rute was born in Puerto Montt, Chile. He received the B.Sc. degree in electrical engineering from University of Chile, Chile, in 2020. Also, he received the M.Sc. degree in electrical engineering from the University of Chile, Chile, in 2020. His research interests include the control of microgrids and model predictive control applied to microgrids.



Alex Navas-Fonseca (S'18) received the B.Sc. degree (Hons.) in electronic engineering from the Army Polytechnic School-ESPE, Ecuador, in 2015. He is currently pursuing a dual PhD degree in electrical and electronic engineering with the University of Nottingham, United Kingdom and the University of Chile, Chile. His research interests include the control and management of microgrids, model predictive control applied to microgrids and renewable energies. He has served as a Reviewer in journals, such as the IEEE Transactions on Smart Grid and IEEE Transactions on Circuits and Systems I.



Juan S. Gómez was born in Bogotá, Colombia. He received the B.E degree in Electronics Engineering from "Universidad Distrital- Francisco José de Caldas", Bogotá, Colombia in 2011, and the Ph.D. degree in Electrical Engineering from the University of Chile (Universidad de Chile), Santiago, Chile in 2020. Dr. Gómez is currently affiliated as postdoctoral researcher on microgrids applications for mining industry at the Pontificia Universidad Católica de Chile (Anillo project ACT192013). He previously worked in the Colombian oil and gas industry as a Project Engineer and as a Specialist Automation Engineer between 2010 and 2016. His research interests are focused mainly on microgrids control, networked control systems, renewable energies, and model-based predictive control.



Enrique Espina (S'17) was born in Santiago, Chile. In 2013, he received the B.Sc. degree in electrical engineering from the University of Santiago of Chile. In 2017, he received the M.Sc. degree in electrical engineering from the University of Chile. In 2021, he received the dual Ph.D. degree in electrical and computer engineering from the University of Waterloo, ON, Canada, and in electrical engineering from the University of Chile, Santiago, Chile. Currently, Mr Espina is an Assistant Professor with the Department of Electrical Engineering at the University of Santiago of Chile, Santiago, Chile. His main research interests include the control of hybrid ac/dc microgrids, energy storage systems, electrical vehicle technologies, renewable energies and power electronic converters.



Claudio Burgos-Mellado (S'17–M'19) was born in Cunco, Chile. He received the B.Sc. and M.Sc. degrees in electrical engineering from the University of Chile, Santiago, Chile, in 2012 and 2013, respectively, and the dual Ph.D. degree in electrical and electronic engineering from the University of Nottingham, U.K., and in electrical engineering from the University of Chile, Santiago, Chile in 2019. From 2019 to 2021, he was a Research Fellow in the Power Electronics, Machines and Control Group (PEMC group) at the University of Nottingham, United Kingdom. Currently, he is an Assistant Professor with the Institute of Engineering Sciences, Universidad de O'Higgins, Rancagua, Chile. His current interests include battery energy storage systems, electrical vehicle technologies, power electronics, microgrids, power quality issues and modular multilevel converters. In 2021, he received the best PhD thesis award in the category of Exact Science from the Chilean Academy of Sciences.



Doris Sáez (S'93–M'96–SM'05) was born in Panguipulli, Chile. She received the M.Sc. and Ph.D. degrees in electrical engineering from the Pontificia Universidad Católica de Chile, Santiago, Chile, in 1995 and 2000, respectively. She is currently a Full Professor with the Department of Electrical Engineering and the Head of the Indigenous People Program, Faculty of Mathematical and Physical Sciences, University of Chile, Santiago. She has coauthored the books *Hybrid Predictive Control for Dynamic Transport Problems* (Springer Verlag, 2013) and *Optimization of Industrial Processes at Supervisory Level: Application to Control of Thermal Power Plants* (Springer-Verlag, 2002). Her research interests include predictive control, fuzzy control design, fuzzy identification, and control of microgrids. She also serves as an Associate Editor for the IEEE Transactions on Smart Grid.



Mark Sumner (SM'05) received the B.Eng degree in Electrical and Electronic Engineering from Leeds University in 1986 and then worked for Rolls Royce Ltd in Ansty, UK. Moving to the University of Nottingham, he completed his PhD in induction motor drives in 1990, and after working as a research assistant, was appointed Lecturer in October 1992. He is now Professor of Electrical Energy Systems. His research interests cover control of power electronic systems including power electronics for enhanced power quality, stability of power electronic converters and novel power system fault location strategies.



Diego Muñoz-Carpintero Received the B.Sc. and M.Sc. degrees in electrical engineering from the Universidad de Chile, in 2009 and 2010, respectively, and the D.Phil. degree in control engineering from the University of Oxford, in 2014. From 2015 to 2016, he was a Research Fellow at Nanyang Technological University, and from 2017 to 2019, he was a Postdoctoral Researcher at the University of Chile. He is currently an Assistant Professor at the Institute of Engineering Science, Universidad de O'Higgins. His research interests include control theory in the areas of predictive, robust and stochastic control; intelligent control; fuzzy and neural modelling; decision making under uncertainty; and their application to energy efficient control of systems such as micro-grids, electric vehicle routing, battery management and agricultural irrigation.